The growth speed of microtubules with XMAP215-coated beads coupled to their ends is increased by tensile force

Anastasiya Trushko[a], Erik Schäffer[b,1,2], and Jonathon Howard[a,2,3]

[a]Max Planck Institute of Molecular Cell Biology and Genetics, 01307 Dresden, Germany; and [b]Biotechnology Center, Technische Universität Dresden, 01307 Dresden, Germany

Edited by J. Richard McIntosh, University of Colorado Boulder, Boulder, CO, and approved July 23, 2013 (received for review October 17, 2012)

The generation of pulling and pushing forces is one of the important functions of microtubules, which are dynamic and polarized structures. The ends of dynamic microtubules are able to form relatively stable links to cellular structures, so that when a microtubule grows it can exert a pushing force and when it shrinks it can exert a pulling force. Microtubule growth and shrinkage are tightly regulated by microtubule-associated proteins (MAPs) that bind to microtubule ends. Given their localization, MAPs may be exposed to compressive and tensile forces. The effect of such forces on MAP function, however, is poorly understood. Here we show that beads coated with the microtubule polymerizing protein XMAP215, the Xenopus homolog of Dis1 and chTOG, are able to link stably to the plus ends of microtubules, even when the ends are growing or shrinking; at growing ends, the beads increase the polymerization rate. Using optical tweezers, we found that tensile force further increased the microtubule polymerization rate. These results show that physical forces can regulate the activity of MAPs. Furthermore, our results show that XMAP215 can be used as a handle to sense and mechanically manipulate the dynamics of the microtubule tip.

microtubule polymerase | microtubule dynamics | optical trap

XMAP215 is a microtubule plus-end binding protein that alters microtubule dynamics (1–4) by promoting microtubule growth. It was identified as a factor increasing microtubule polymerization rates in *Xenopus* egg extracts (5). In vivo studies have shown that disruption of XMAP215 function leads to short interphase microtubules, reduced microtubule growth rate, and increased frequency of microtubule catastrophe and pause events (6–11). Depletion of XMAP215 also results in short, abnormally formed mitotic spindles and short astral microtubules (7, 12, 13). In vitro studies have demonstrated that XMAP215 binds preferentially to the microtubule plus end and follows the growth and shrinkage of the microtubule tip, catalyzing microtubule growth (14–16). In addition to localization at the microtubule plus end and centrosomes (17–19), proteins of the XMAP215/Dis1 family are found at the kinetochores (9, 20, 21), which are sites of high force during cell division. Microtubules themselves can exert pulling and pushing forces (22–30). Therefore, the localization of XMAP215 at microtubule ends suggests that XMAP215 can function under load. However, the effect of forces on XMAP215 activity has not been directly analyzed. In this study, we investigated the influence of forces—directed toward the microtubule plus and minus end—on XMAP215 activity in vitro. Microtubule growth and shrinkage were monitored with high spatial and temporal resolution by visualizing the position of XMAP215-coated polystyrene microspheres bound to the tips of dynamic microtubules. The microspheres, so-called "beads," served as handles to apply forces on XMAP215 molecules using optical tweezers.

Results

XMAP215-Coated Beads Remain Attached to Growing and Shrinking Microtubule Ends. To test whether XMAP215-coated beads recognize and bind microtubule tips, we reconstituted the interaction of XMAP215 molecules with dynamic microtubule ends. For this purpose, rhodamine-labeled microtubule seeds were attached to a coverslip via antirhodamine antibodies. Upon addition of a solution containing unlabeled tubulin protein and XMAP215-coated beads, the microtubule seeds started to grow dynamic extensions. XMAP215 was coupled to the beads via its C terminus (*Materials and Methods*); with this geometry, the N-terminal, tubulin-binding tumor overexpressed gene (TOG) domains (16) have access to the microtubule. The dynamics were characterized by alternating periods of growth and shrinkage. Beads were trapped using optical tweezers (31–34), brought into the vicinity of the growing end of a microtubule, and then positioned on it to allow binding to occur. When the optical trap was switched off, the bound XMAP215-coated bead remained attached to the microtubule tip. To quantify the movement of the beads due to microtubule growth and shrinkage, we recorded differential interference contrast (DIC) (33) movies and tracked the position of the bead (Fig. 1*A*). The resulting bead trajectory was calculated from the tracked position and decomposed into movement parallel (Fig. 1*B*, *Upper*) and perpendicular (Fig. 1*B*, *Lower*) to the microtubule axis. The motion was the superposition of the directed movement due to microtubule growth and shrinkage and higher frequency fluctuations, perhaps due to Brownian motion of the XMAP215-coated bead, and thermally induced bending of the flexible microtubule extension. XMAP215-coated beads remained attached to the dynamic microtubule tip for 472 ± 95 s (mean $\pm$ SE unless noted otherwise, $N = 21$) in the presence of 15 μM of tubulin at 29 °C (Fig. 1*C*). During microtubule growth, the beads moved 7.0 ± 1.3 μm ($N = 17$) before they either detached or switched to shrinkage-driven movement. Microtubule shrinkage led to movement over 7.9 ± 1.5 μm ($N = 11$) (Fig. 1*D*). These results show that XMAP215-coated beads can remain attached to growing and shrinking microtubule ends. Because the attachment times are much longer than those measured using single-molecule fluorescence (~2 s) (15), the microtubule end is likely interacting with a large number of XMAP215 molecules at the bead surface. Given the geometry of the bead, it is possible that every protofilament end is interacting with an XMAP215 molecule (*Materials and Methods*).

XMAP215-Coated Beads Increase Microtubule Growth Speed. To assess the microtubule polymerization activity of XMAP215-coated

Author contributions: A.T., E.S., and J.H. designed research; A.T. performed research; A.T., E.S., and J.H. analyzed data; and A.T., E.S., and J.H. wrote the paper.

The authors declare no conflict of interest.

This article is a PNAS Direct Submission.

Freely available online through the PNAS open access option.

[1]Present address: Center for Plant Molecular Biology, University of Tübingen, D-72076 Tübingen, Germany.

[2]To whom correspondence may be addressed. E-mail: Jonathon.Howard@Yale.edu or erik.schaeffer@uni-tuebingen.de.

[3]Present address: Department of Molecular Biophysics & Biochemistry, Yale University, New Haven, CT 06520.

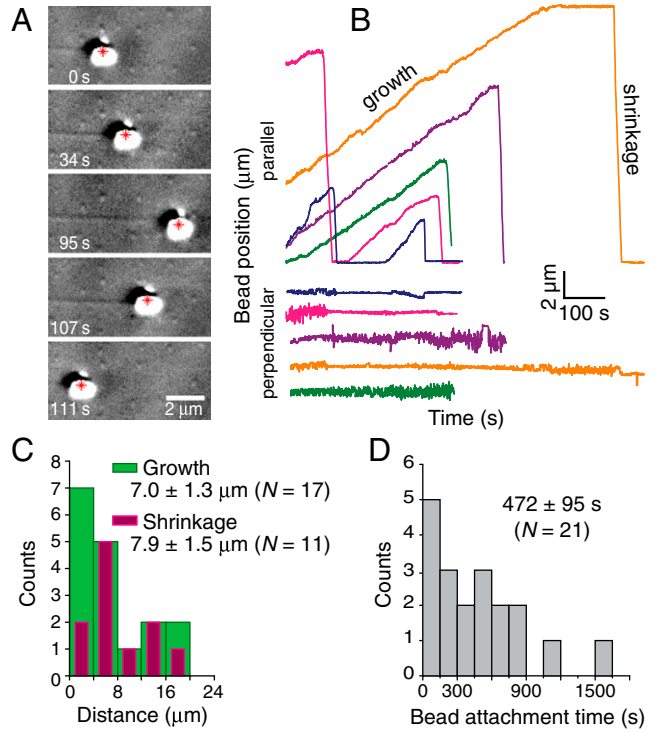

Fig. 1. XMAP215-coated beads track microtubule tips. (*A*) Selected frames from a DIC movie of an XMAP215-coated bead being moved by a growing and shrinking microtubule end. The red cross indicates the tracked position of the bead. (*B*) Records of XMAP215-coated bead position parallel (*Upper*) and perpendicular (*Lower*) to the direction of the microtubule axis versus time during growth and shrinkage. (*C*) Histogram of the distances over which the XMAP215-coated beads moved during microtubule growth and shrinkage. (*D*) Histogram of the bead attachment times at the microtubule tip during both growth and shrinkage. Note that shrinkage times do not contribute much to the total time.

beads, we quantified their effect on microtubule dynamics by comparing the speed of microtubule growth and shrinkage with and without XMAP215-coated beads on their tips. Growth and shrinkage speeds of microtubules not interacting with XMAP215-coated beads were calculated from kymographs (Fig. 2 *A*–*C*). In the same field of view, the corresponding speeds of microtubules attached to beads were calculated from linear fits to the tracked movement (see Fig. 1*B* for example tracks). Our results show that attachment of XMAP215-coated beads was associated with nearly a twofold increase in microtubule growth speed (Fig. 2*D*). For a single bead, this increase is remarkable considering that for saturating XMAP215 concentrations only a fivefold increase was reported (15). In contrast, the shrinkage speed remained unchanged (Fig. 2*E*). Also, times until a catastrophe occurred were unchanged:7.2 ± 0.5 min ($N = 247$ catastrophes, mean ± mean/$\sqrt{N}$) without beads and 8 ± 2 min ($N = 13$ catastrophes) with beads. These results show that XMAP215 retains its polymerization activity in our in vitro assay.

XMAP215 Molecules Are Able to Maintain Contact to a Growing Microtubule End in the Presence of Minus-End–Directed Forces. To determine whether XMAP215-coated beads are able to support load and remain attached to the dynamic microtubule end, we applied an increasing minus-end-directed force to the microtubule by holding the bead in a stationary optical trap (Fig. 3*A*). When the microtubule tip grew, the bead was displaced from the center of the optical trap and was subjected to an increasing restoring force directed toward the minus end of the microtubule. Eventually, the XMAP215-coated bead detached from the microtubule tip very rapidly and returned to the center of the trap (Fig. 3*B*). The bead's speed following detachment was much faster than the speed of shortening following catastrophe, allowing us to distinguish between these two cases. To quantify the detachment force, the bead was monitored by back-focal-plane interferometry (35, 36). Based on this analysis, the mean detachment force of the XMAP215-coated beads was 1.0 ± 0.1 pN ($N = 18$), with maximum forces up to 2.5 pN (Fig. 3*C*). These results indicate that XMAP215 molecules are able to maintain contact to a growing microtubule end in the presence of minus-end-directed forces up to a few pN.

Tensile Forces Enhance Microtubule Polymerization Activity of XMAP215. To determine whether the XMAP215 microtubule polymerization activity is force sensitive, we used the optical trap to apply steady forces to XMAP215-coated beads coupled to microtubule tips (Fig. 4*A*). The applied forces were 0.5 pN and 1 pN toward the plus end (in the direction of growth) and −0.5 pN toward the minus end (in the direction of shrinkage); the force was kept constant by using a feedback-controlled mirror to move the position of the optical trap and maintain a fixed offset between the bead and the trap center. To quantify the XMAP215-coated bead movement parallel to the microtubule axis, we fitted a line to the corresponding displacement of the bead (Fig. 4*B*), $x = \upsilon t + x_0$, where x is the position, υ the speed, t the time, and x_0 the initial position of the bead at $t = 0$ s. To determine the influence of applied forces on the bead movements, we plotted the bead's growth speed (Fig. 4*C*), the time to catastrophe (Fig. 4*D*), and the shrinkage speed (Fig. 4*E*) against the applied forces. The time to catastrophe and the shrinkage speed were independent of force: the average time to catastrophe was 2.6 ± 0.4 min ($N = 49$) corresponding to a catastrophe frequency of 0.0064 ± 0.0010 s^{-1}; the mean shrinkage speed was 43 ± 4 μm/min ($N = 49$), consistent with Fig. 2*E*. We did not observe any rescue events. These values are consistent with the literature (37, 38). The zero-force growth speed was smaller than the speeds reported in the other figures because, in the constant-force experiments, we used a lower tubulin concentration (7.5 μM).

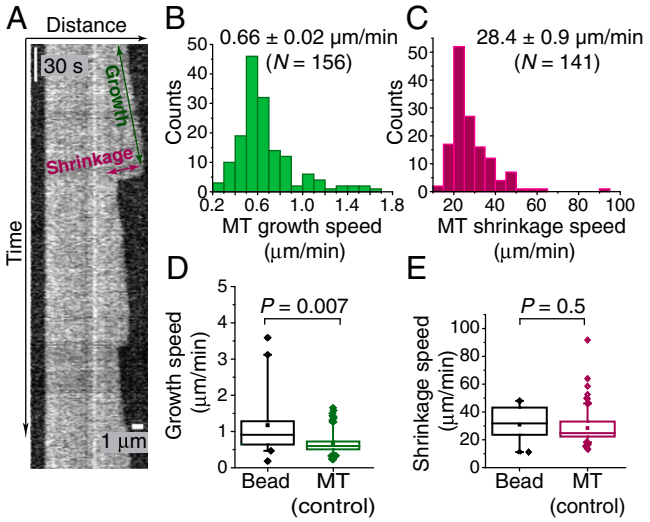

Fig. 2. XMAP215-coated beads accelerate microtubule growth. (*A*) A representative kymograph of a microtubule. Growth and shrinkage phases are indicated. (*B*) Histogram of the microtubule (MT) growth speeds. (*C*) Histogram of MT shrinkage speeds. (*D*) Box plots of MT growth speeds when attached to a bead [mean ± SE: 1.1 ± 0.2 μm·min^{-1} ($N = 17$), black] and when not attached [0.66 ± 0.02 μm·min^{-1} ($N = 156$), green]. (*E*) Box plots of MT shrinkage speeds when attached to a bead [33 ± 4 μm·min^{-1} ($N = 11$), black] and when not attached [28.4 ± 0.9 μm·min^{-1} ($N = 141$), magenta].

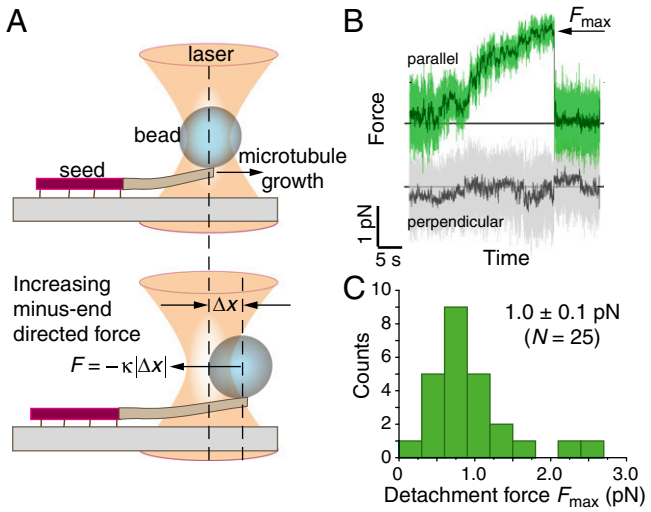

Fig. 3. XMAP215-coated beads remain attached to growing microtubule tips subjected to minus-end-directed forces. (*A*) Schematic of the bead assay with a stationary trap (not to scale): as the microtubule grows, the bead displacement from the trap center Δx increases, increasing the opposing, minus-end-directed force $F = -\kappa|\Delta x|$, where κ is the trap stiffness. (*B*) Force on the bead in the direction of the microtubule axis (parallel, green) and perpendicular to it [gray; raw data (dim), adjacent averaging over 200 data points (dark)]. Horizontal lines correspond to zero force when $\Delta x = 0$. (*C*) Histogram of the maximum minus-end–directed forces supported by XMAP215-coated beads.

We reduced the concentration to slow growth and lower the microtubule lengths, thereby minimizing microtubule bending fluctuations. For the smaller forces, −0.5 pN, 0 pN, and +0.5 pN, the growth speeds clustered around 0.77 ± 0.06 μm/min ($N = 56$, Fig. 4*C*). However, at a plus-end-directed force of 1 pN, the mean speed was 1.34 ± 0.16 μm/min ($N = 16$), which was significantly higher than the speed at smaller forces ($P < 0.005$, Welch's unpaired *t* test). Thus, a positively directed force increased the rate of microtubule growth in the presence of XMAP215.

Discussion

We have shown that beads coated with XMAP215 are able to maintain contact with growing and shrinking microtubules while they grow and shrink by several micrometers. The ability of the growing and shrinking ends of the microtubules to move a cargo in vivo appears to be dependent upon linker molecules. For instance, the kinetochores maintain persistent attachment of the depolymerizing microtubule plus ends to the chromosomes, enabling chromosome segregation during cell division. According to our results, XMAP215 is a candidate for such a linker protein, as XMAP215-coated beads remained attached to the growing and shrinking microtubule ends over long distances, with growth times up to several minutes. Such highly processive motion could be explained both by the ability of XMAP215 to recognize, bind, and track the dynamic microtubule plus end (15) and by the interaction of several XMAP215 molecules tethered to a polystyrene bead providing stable attachment of the cargo to the microtubule tip. The same cargo-coupling abilities to the depolymerizing microtubule end have been shown for the Dam1 complex (39) and Ndc80 (40), which are part of the kinetochore complex (41) and are known to be load-bearing proteins during chromosome segregation. Recently, such a linker property has also been shown for the microtubule depolymerase MCAK (42), which is localized to the kinetochores during cell division as well as cytoplasmic dynein (43). Thus, XMAP215 is one of several proteins capable of coupling to the microtubule ends under load.

XMAP215-coated beads were able to increase the growth rate of microtubules, showing that XMAP215 retains its polymerase activity when coupled to the beads. We have shown that the growth rate is further increased by a 1 pN force directed toward the plus end of the microtubule (i.e., in the direction of growth). Such a force will put both the XMAP215 proteins and the microtubule itself under tension. What is the mechanism underlying this increase in growth rate? Previous in vitro studies have shown that XMAP215 acts as a catalytic activator (15, 16). According to this model, the microtubule end can be thought of as an enzyme that catalyzes the transfer of a tubulin dimer from the unpolymerized state (free in the solution) to the polymerized state (incorporated into the microtubule lattice). XMAP215, by binding to the end, lowers the energy of the transition state (a tubulin dimer weakly bound at the microtubule end), thereby accelerating the rate of addition of free dimers into the microtubule. The activity of XMAP215 is determined by its v_{max}, the maximum growth acceleration when the end is saturated with

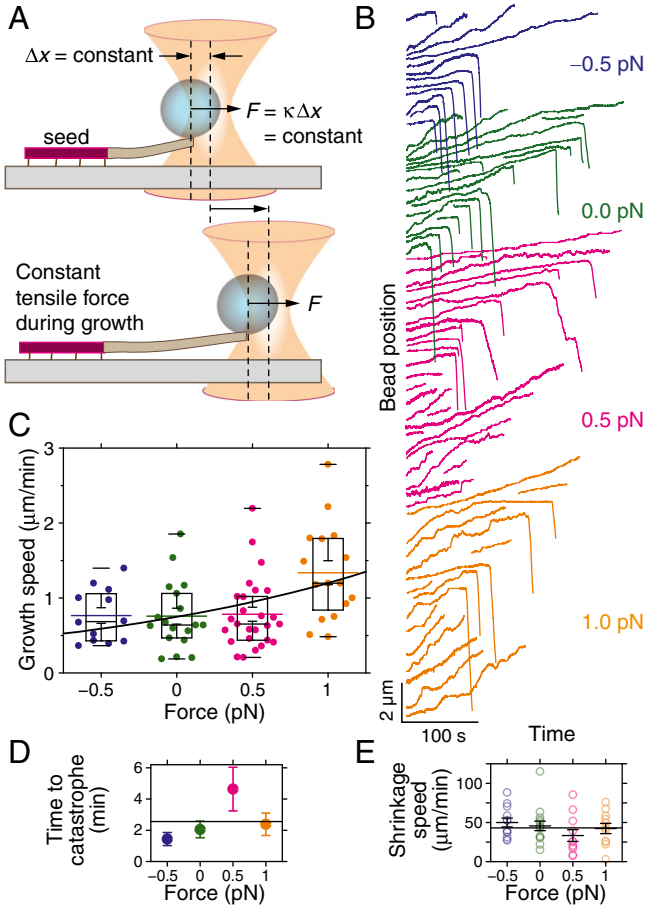

Fig. 4. XMAP215 polymerization activity is enhanced by tensile force. (*A*) Schematic of a constant tensile force experiment in the direction of microtubule growth. (*B*) Records of the positions of XMAP215-coated beads coupled to microtubule tips with different applied load forces versus time. (*C*) Microtubule growth speed versus applied force. Colored horizontal lines and whiskers on the box plot indicate the mean and SE of the data, respectively. Black horizontal lines indicate the maximum and minimum. Data points (colored dots) are offset in force for clarity. The solid line is an exponential fit, $v(F) = v_0 \exp(Fx_0/k_BT)$, to all data (see *Discussion*). (*D*) Time to catastrophe versus force (mean ± mean/$\sqrt{N}$), with the average indicated by the line. (*E*) Shrinkage speed versus force (black line symbols, mean ± SE; open colored circles, individual data points). The horizontal line is the average. In *C*, there were 12, 18, 26, and 16, and in *D* and *E*, 12, 15, 11, and 11 data points for −0.5, 0, 0.5, and 1 pN, respectively.

XMAP215, and the K_M, the XMAP215 concentration at which the end is 50% saturated with XMAP215 (16). A tensile force could accelerate growth by increasing the activity of XMAP215 through an increase in v_{max} or a decrease in K_M.

The simplest model is that a tensile force acting on the beads decreases K_M by pulling XMAP215 molecules to the microtubule end and, therefore, increases the probability that the terminal tubulin dimer is occupied by XMAP215 (where it can participate in catalysis). For example, if an XMAP215-coated bead can diffuse on the microtubule surface, as can single molecules of XMAP215 (15), and if, in the absence of force, the effective concentration of XMAP215 at the end is below the K_M for catalytic activation, then a constant tensile force will influence the probability, $p(\ell)$, of finding the bead a distance ℓ away from the microtubule end according to a Boltzmann distribution: $p(\ell) = p_0 \exp(-F\ell/(k_B T))$, where k_B is the Boltzmann constant and T the temperature. In this case, tensile force will increase the growth rate exponentially. Such exponential growth is consistent with the data. Fitting $v(F) = v_0 \exp(Fx_0/k_B T)$ to the data (Fig. 4*C*, solid line) resulted in a microtubule growth speed in the absence of force of $v_0 = 0.75 \pm 0.08$ μm·min^{-1} and a characteristic length of $x_0 = 2.0 \pm 0.6$ nm (mean ± SE; x_0 significantly different from zero with $t = 3.32$, $N = 72$, and $P = 0.0014$). The value of x_0 is intermediate between the length of the dimer (8 nm) and the average increase in microtubule length upon dimer addition (8 nm/13 ≈ 0.6 nm, for a 13-protofilament microtubule). Thus, a mechanism by which tensile force concentrates XMAP215 at the microtubule end accords with the data.

An alternative model is that a tensile force acting on the beads increases v_{max} by making XMAP215 a more effective polymerase. For example, if the unbinding of the TOG domain from the newly incorporated tubulin dimer is rate limiting in the absence of force, then a tensile force could accelerate the unbinding by unpeeling XMAP215 from the microtubule wall, thereby accelerating polymerization. In this picture, the characteristic length of 2.0 nm could be interpreted as the transition state for TOG unbinding. An argument against this mechanism is that XMAP215 is attached to the bead via its C terminus, yet the polymerase activity is primarily due to the first two TOG domains, located at the N terminus (16); thus, the effect on these TOG domains of forces exerted through the bead will be diminished if the intervening three TOG domains (and the basic domain) bind to the microtubule. The specific model of Ayaz et al. (44) proposes that the most-N-terminal TOG domain (TOG1) catalyzes subunit incorporation, whereas TOG2 helps to maintain attachment to the microtubule end; a tensile force applied through the C terminus would not be expected to accelerate polymerization in this model. For this reason, we prefer the diffusion mechanism; although because the spatial arrangement of the TOG domains at the microtubule end is not known for sure, the possibility that tensile force increases v_{max} cannot, at present, be excluded.

A third possibility is that a tensile force induces a structural change at the microtubule end that facilitates polymerization (45–49). For example, if the protofilaments are curved at the microtubule end, a tensile force will tend to straighten the protofilament and this may facilitate the incorporation of a "bent" dimer into the straight lattice (46, 48). However, we estimate that a 1 pN force will have only a very modest effect on the curvature of a protofilament, $\lesssim 1$ degree per tubulin dimer (using the flexural rigidity of a single protofilament used in ref. 49 of $5 \cdot 10^{-27}$ N·m^{-2} and assuming a protofilament length of up to five tubulin dimers). Therefore, the hypothesis that force is influencing the growth rate through protofilament straightening appears less likely to explain the observed effects.

In summary, our results show that XMAP215 dynamically links to the ends of growing and shrinking microtubules. XMAP215 accelerates microtubule growth, and we show that it retains its polymerase activity when coupled to a bead. Furthermore, we provide evidence that mechanical force can increase the polymerization activity. These results provide insights into the mechanism of XMAP215-mediated acceleration of microtubule growth. Given the cellular localization of XMAP215, this mechanical activation could play a role in processes such as cell division when the microtubule plus ends are in contact with the chromosomal kinetochores. However, further studies will be required to determine whether XMAP215 molecules actually function under tension in the cell.

Materials and Methods

Tubulin and Microtubule Preparation. Porcine brain tubulin was purified as described (50). Labeling of cycled tubulin with tetramethylrhodamine (Invitrogen) was performed as reported in ref. 51. GMPCPP-stabilized microtubules were grown according to ref. 51.

XMAP215–GFP–His$_7$ Expression and Purification. Full-length XMAP215–GFP–His$_7$ was expressed and purified as described previously (15, 16).

Coupling of XMAP215–GFP–His$_7$ to Polystyrene Microspheres. The protein XMAP215–GFP–His$_7$ was immobilized on the surface of a 0.59-μm-diameter carboxylated polystyrene microsphere (Bangs Laboratories, product no. PC03N/6487) through a linker consisting of a polyethylene glycol (PEG) molecule and an antibody specific to GFP. Two types of the PEG-molecules of different molecular weight, α-Methoxy-ω-amino PEG of 2 kDa (product no. 12 2000–2, Rapp Polymere GmbH), further referred to as NH_2–PEG–CH_3O, and α-Amino-ω-carboxyl PEG hydrochloride of 3 kDa (product no. 13 3000–20-32, Rapp Polymere GmbH), further referred to as NH_2–PEG–COOH, were covalently attached to the microsphere surface in a 9:1 ratio, respectively. Such a mixture prevented particle aggregation because of the hydrophilic properties of the 2 kDa PEG molecules. Furthermore, we could covalently couple a GFP antibody via the carboxyl group of the 3 kDa PEG molecules and the amino groups of the antibodies. For the PEG molecule coupling, 25 μL carboxyl-modified microspheres were pelleted two times in 1,000 μL of 50 mM Mes pH 6.0 at 13,000 *g* for 3 min and resuspended in 250 μL of 50 mM Mes pH 6.0. To activate the COOH groups on the microspheres, 1.62 mg of *N*-hydroxysulfosuccinimide sodium salt [sulfo-NHS, 56485–98.5% (HPLC), Sigma-Aldrich] and 1.42 mg of *N*-(3-dimethylaminopropyl)-N′-ethyl-carbodiimide hydrochloride (EDC, 130672–98%, Sigma-Aldrich) were added sequentially. The particles were incubated in a thermoshaker at 600 rpm, at 37 °C for 15 min. After the incubation, the microspheres were washed two times in 500 μL 50 mM Mes pH 6.0 to get rid of nonreacted sulfo-NHS and EDC. The beads were resuspended in the PEG solution (9.36 mg of 2 kDa NH_2–PEG–CH_3O and 1.56 mg of 3 kDa NH_2–PEG–COOH in borate buffer pH 8.5) with an incubation in the thermoshaker at 600 rpm, at 37 °C for 2 h. After the incubation time, the particles were washed five times in 500 μL of borate buffer pH 8.5, three times in 500 μL of 50 mM Mes pH 6.0, and resuspended in 250 μL of 50 mM Mes pH 6.0 for the subsequent second step of covalent coupling of antibodies specific to GFP. During the second step of the coupling protocol, 250 μL PEG-coated microspheres in 50 mM Mes pH 6.0 were activated a second time by the addition of 1.62 mg of sulfo-NHS and 1.42 mg of EDC and incubated in the thermoshaker at 600 rpm, at 37 °C for 15 min. After the activation, the microspheres were washed two times in 500 μL of 50 mM Mes pH 6.0, resuspended in 250 μL of antibody solution (45 μg monoclonal mouse antibody specific to GFP in 1× PBS), and incubated in the thermoshaker at 600 rpm, at 37 °C for 1 h and then at 600 rpm, at 4 °C overnight. Then the microspheres were washed five times in 1× PBS and stored at 4 °C before the XMAP215–GFP–His$_7$ coupling step. To immobilize XMAP215–GFP–His$_7$ molecules on a polystyrene microsphere via the GFP-tag, 47 μg of the modified polystyrene microspheres were incubated with an XMAP215 solution (96 nM XMAP215–GFP–His$_7$, 10 mM Tris Base, 10 mM Bis·Tris, 100 mM KCl, 1 mM DTT) in the thermoshaker at 600 rpm, at 4 °C overnight. XMAP215–GFP–His$_7$ was freshly purified and not frozen before this step. Then, after addition of 10% (vol/vol) glycerol, the XMAP215–GFP–His$_7$ coupled microspheres were aliquoted, snap frozen in liquid nitrogen, and stored at –80 °C. To test if the PEG molecules were bound to the surface of the beads, we incubated beads with and without conjugated PEGs with fluorescently labeled BSA. Because a PEG coating reduces nonspecific binding, the fluorescent signal of surface-conjugated PEG beads was lower than the one of the control beads without any PEGs. Also, PEG-coated microspheres that were used without XMAP215 did not show any interaction with microtubules or the flow-cell surface. After all preparation steps, the PEG-antibody beads were fluorescent after incubation with XMAP215–GFP.

Given the ratio of beads to XMAP215 in the final coupling reaction, there are at most 16,000 XMAP215 molecules per bead assuming 100% binding and no losses. Because of the geometry of the experiment, no more than 10% and 1% of the molecules ($N < 1600$ and $N < 160$, respectively) could interact simultaneously with the microtubule lattice and end, respectively. These numbers may greatly overestimate the real numbers.

Assay Conditions. The preparation of silanized cover glasses and chamber preparation was previously described (15, 34, 51). Reaction channels were first rinsed with BRB80: 80 mM Pipes at pH 6.9, 1 mM $MgCl_2$, and 1 mM EGTA. Reaction channels were incubated with 1% antirhodamine antibody (Invitrogen) in BRB80 for 10 min, followed by 1% Pluronic F127 (Sigma) in BRB80 for 10 min, and rhodamine-labeled GMPCPP-stabilized microtubule seeds for 5 min. To reconstitute microtubule growth, the tubulin solution together with XMAP215-coated microspheres were introduced into the channel, 15 μm tubulin for both DIC microtubule growth observation and XMAP215-coated bead detachment-force measurements, and 7.5 μm of tubulin for constant-force experiments (the buffer contained BRB80, 15 or 7.5 μM tubulin, 42.5 μM D-glucose, 42.5 μg/mL glucose oxidase, 17 μg/mL catalase, 10.5 mM DTT, 85 μg/mL casein, 1.25 mM GTP, 75 mM KCl, 80 times diluted XMAP215-coated microspheres). The temperature during the experiments was 29.3 °C. Very few beads interacted with the microtubule lattice by themselves because the bead concentration was low and the basic, microtubule-lattice binding domain, located toward the C terminus, might have been masked by the proximity to the bead and neighboring molecules.

Instrumentation and Data Collection. To quantify the movement of the beads due to microtubule growth and shrinkage, we recorded DIC movies at 30 Hz, averaged over 10 frames, resulting in 3 frames per second. The implementation of video-enhanced DIC using a light-emitting diode was described previously (33). Bead positions were tracked in recorded movies by using a custom-written MATLAB script. Two optical tweezer setups were used. For assays with increasing load, a stationary trap, described in ref. 32, was used. The setup for constant-force experiments was described in ref. 52. In both setups, the position of the bead was monitored by back–focal-plane interferometry (35, 36). The trap stiffness was calibrated along three principal axis as described (31). During constant-force measurements, the bead position was sampled at 40 kHz, averaged over 10 neighboring data points, and recorded at 4 kHz, whereas the mirror position was updated at 1 kHz to maintain a desired load. For stationary trap experiments, the bead position was sampled at 5 kHz. The trap stiffness was about 0.04 pN/nm in the direction of the microtubule axis and 0.026 pN/nm perpendicular to it. For the constant-force experiments, we obtained a total of 130 runs where the bead moved with the end of a growing and/or shrinking microtubule. For analysis of growth speed on force, we applied the following two criteria to the data: (*i*) the duration of the recording exceeded 20 s (chosen to ensure that there was ample time for the bead to couple to the end of the microtubule and that the displacement was comparable to the radius of the 0.59-μm-diameter bead), and (*ii*) the speed exceeded 2.3 nm/s (0.14 μm/min), below which we regarded the bead as immobile. With these criteria, the number of traces included in the growth-speed analysis was 72 and are plotted in Fig. 4*B*. All traces that included a transition to shrinkage (43) were used to calculate the shrinkage speed and the catastrophe rate.

ACKNOWLEDGMENTS. We thank Volker Bormuth for scientific discussions, sharing the MATLAB scripts, developing the optical trap setup, and bead optimization; Mohammed Mahamdeh for developing the optical trap setup and technical support; Per Widlund and Heike Petzold for help with XMAP215 expression and purification; Horatiu Fontana for sharing his bead protocol; Anita Jannasch for some bead controls; and Iain Patten for the paper draft reviewing. The work was supported by the European Community's Seventh Framework Programme (FP7/2007-2013) under Grant Agreement 241548 (MitoSys Project), the Deutsche Forschungsgemeinschaft (Emmy Noether Program), European Research Council (ERC Starting Grant 2010, Nanomech 260875), the Technische Universität Dresden, and the Universität Tübingen.

1. Mitchison T, Kirschner M (1984) Dynamic instability of microtubule growth. *Nature* 312(5991):237–242.
2. Cassimeris L, Pryer NK, Salmon ED (1988) Real-time observations of microtubule dynamic instability in living cells. *J Cell Biol* 107(6 Pt 1):2223–2231.
3. Sammak PJ, Borisy GG (1988) Direct observation of microtubule dynamics in living cells. *Nature* 332(6166):724–726.
4. Belmont LD, Hyman AA, Sawin KE, Mitchison TJ (1990) Real-time visualization of cell cycle-dependent changes in microtubule dynamics in cytoplasmic extracts. *Cell* 62(3): 579–589.
5. Gard DL, Kirschner MW (1987) A microtubule-associated protein from Xenopus eggs that specifically promotes assembly at the plus-end. *J Cell Biol* 105(5):2203–2215.
6. Wang PJ, Huffaker TC (1997) Stu2p: A microtubule-binding protein that is an essential component of the yeast spindle pole body. *J Cell Biol* 139(5):1271–1280.
7. Cullen CF, Deák P, Glover DM, Ohkura H (1999) Mini spindles: A gene encoding a conserved microtubule-associated protein required for the integrity of the mitotic spindle in Drosophila. *J Cell Biol* 146(5):1005–1018.
8. Tournebize R, et al. (2000) Control of microtubule dynamics by the antagonistic activities of XMAP215 and XKCM1 in Xenopus egg extracts. *Nat Cell Biol* 2(1):13–19.
9. Garcia MA, Vardy L, Koonrugsa N, Toda T (2001) Fission yeast ch-TOG/XMAP215 homologue Alp14 connects mitotic spindles with the kinetochore and is a component of the Mad2-dependent spindle checkpoint. *EMBO J* 20(13):3389–3401.
10. Brittle AL, Ohkura H (2005) Mini spindles, the XMAP215 homologue, suppresses pausing of interphase microtubules in Drosophila. *EMBO J* 24(7):1387–1396.
11. Kawamura E, Wasteneys GO (2008) MOR1, the Arabidopsis thaliana homologue of Xenopus MAP215, promotes rapid growth and shrinkage, and suppresses the pausing of microtubules in vivo. *J Cell Sci* 121(Pt 24):4114–4123.
12. Gergely F, Draviam VM, Raff JW (2003) The ch-TOG/XMAP215 protein is essential for spindle pole organization in human somatic cells. *Genes Dev* 17(3):336–341.
13. Cassimeris L, Morabito J (2004) TOGp, the human homolog of XMAP215/Dis1, is required for centrosome integrity, spindle pole organization, and bipolar spindle assembly. *Mol Biol Cell* 15(4):1580–1590.
14. Kerssemakers JWJ, et al. (2006) Assembly dynamics of microtubules at molecular resolution. *Nature* 442(7103):709–712.
15. Brouhard GJ, et al. (2008) XMAP215 is a processive microtubule polymerase. *Cell* 132(1):79–88.
16. Widlund PO, et al. (2011) XMAP215 polymerase activity is built by combining multiple tubulin-binding TOG domains and a basic lattice-binding region. *Proc Natl Acad Sci USA* 108(7):2741–2746.
17. Lee MJ, Gergely F, Jeffers K, Peak-Chew SY, Raff JW (2001) Msps/XMAP215 interacts with the centrosomal protein D-TACC to regulate microtubule behaviour. *Nat Cell Biol* 3(7):643–649.
18. Bellanger JM, Gönczy P (2003) TAC-1 and ZYG-9 form a complex that promotes microtubule assembly in C. elegans embryos. *Curr Biol* 13(17):1488–1498.
19. Kinoshita K, et al. (2005) Aurora A phosphorylation of TACC3/maskin is required for centrosome-dependent microtubule assembly in mitosis. *J Cell Biol* 170(7):1047–1055.
20. Tanaka K, et al. (2005) Molecular mechanisms of kinetochore capture by spindle microtubules. *Nature* 434(7036):987–994.
21. Kitamura E, et al. (2010) Kinetochores generate microtubules with distal plus ends: Their roles and limited lifetime in mitosis. *Dev Cell* 18(2):248–259.
22. Inoué S, Salmon ED (1995) Force generation by microtubule assembly/disassembly in mitosis and related movements. *Mol Biol Cell* 6(12):1619–1640.
23. Yeh E, et al. (2000) Dynamic positioning of mitotic spindles in yeast: Role of microtubule motors and cortical determinants. *Mol Biol Cell* 11(11):3949–3961.
24. Doe CQ, Bowerman B (2001) Asymmetric cell division: Fly neuroblast meets worm zygote. *Curr Opin Cell Biol* 13(1):68–75.
25. Tran PT, Marsh L, Doye V, Inoué S, Chang F (2001) A mechanism for nuclear positioning in fission yeast based on microtubule pushing. *J Cell Biol* 153(2):397–411.
26. Gönczy P (2002) Mechanisms of spindle positioning: Focus on flies and worms. *Trends Cell Biol* 12(7):332–339.
27. Kusch J, Meyer A, Snyder MP, Barral Y (2002) Microtubule capture by the cleavage apparatus is required for proper spindle positioning in yeast. *Genes Dev* 16(13): 1627–1639.
28. Howard J, Hyman AA (2003) Dynamics and mechanics of the microtubule plus end. *Nature* 422(6933):753–758.
29. Liakopoulos D, Kusch J, Grava S, Vogel J, Barral Y (2003) Asymmetric loading of Kar9 onto spindle poles and microtubules ensures proper spindle alignment. *Cell* 112(4): 561–574.
30. Maekawa H, Usui T, Knop M, Schiebel E (2003) Yeast Cdk1 translocates to the plus end of cytoplasmic microtubules to regulate bud cortex interactions. *EMBO J* 22(3): 438–449.
31. Tolic-Norrelykke S, Schäffer E, Howard J (2006) Calibration of optical tweezers with positional detection in the back focal plane. *Rev Sci Instrum* 77:103101.
32. Schäffer E, Nørrelykke SF, Howard J (2007) Surface forces and drag coefficients of microspheres near a plane surface measured with optical tweezers. *Langmuir* 23(7): 3654–3665.
33. Bormuth V, Howard J, Schäffer E (2007) LED illumination for video-enhanced DIC imaging of single microtubules. *J Microsc* 226(Pt 1):1–5.
34. Bormuth V, Varga V, Howard J, Schäffer E (2009) Protein friction limits diffusive and directed movements of kinesin motors on microtubules. *Science* 325(5942):870–873.
35. Gittes F, Schmidt CF (1998) Interference model for back-focal-plane displacement detection in optical tweezers. *Opt Lett* 23(1):7–9.
36. Pralle A, Prummer M, Florin EL, Stelzer EH, Hörber JK (1999) Three-dimensional high-resolution particle tracking for optical tweezers by forward scattered light. *Microsc Res Tech* 44(5):378–386.
37. Walker RA, et al. (1988) Dynamic instability of individual microtubules analyzed by video light microscopy: Rate constants and transition frequencies. *J Cell Biol* 107(4): 1437–1448.
38. Fygenson DK, Braun E, Libchaber A (1994) Phase diagram of microtubules. *Phys Rev E Stat Phys Plasmas Fluids Relat Interdiscip Topics* 50(2):1579–1588.

39. Asbury CL, Gestaut DR, Powers AF, Franck AD, Davis TN (2006) The Dam1 kinetochore complex harnesses microtubule dynamics to produce force and movement. *Proc Natl Acad Sci USA* 103(26):9873–9878.
40. Powers AF, et al. (2009) The Ndc80 kinetochore complex forms load-bearing attachments to dynamic microtubule tips via biased diffusion. *Cell* 136(5):865–875.
41. Akiyoshi B, et al. (2010) Tension directly stabilizes reconstituted kinetochore-microtubule attachments. *Nature* 468(7323):576–579.
42. Oguchi Y, Uchimura S, Ohki T, Mikhailenko SV, Ishiwata S (2011) The bidirectional depolymerizer MCAK generates force by disassembling both microtubule ends. *Nat Cell Biol* 13(7):846–852.
43. Laan L, et al. (2012) Cortical dynein controls microtubule dynamics to generate pulling forces that position microtubule asters. *Cell* 148(3):502–514.
44. Ayaz P, Ye X, Huddleston P, Brautigam CA, Rice LM (2012) A TOG:αβ-tubulin complex structure reveals conformation-based mechanisms for a microtubule polymerase. *Science* 337(6096):857–860.
45. Janson ME, de Dood ME, Dogterom M (2003) Dynamic instability of microtubules is regulated by force. *J Cell Biol* 161(6):1029–1034.
46. Wang HW, Nogales E (2005) Nucleotide-dependent bending flexibility of tubulin regulates microtubule assembly. *Nature* 435(7044):911–915.
47. Franck AD, et al. (2007) Tension applied through the Dam1 complex promotes microtubule elongation providing a direct mechanism for length control in mitosis. *Nat Cell Biol* 9(7):832–837.
48. Rice LM, Montabana EA, Agard DA (2008) The lattice as allosteric effector: Structural studies of alphabeta- and gamma-tubulin clarify the role of GTP in microtubule assembly. *Proc Natl Acad Sci USA* 105(14):5378–5383.
49. Grishchuk EL, Molodtsov MI, Ataullakhanov FI, McIntosh JR (2005) Force production by disassembling microtubules. *Nature* 438(7066):384–388.
50. Gell C, et al. (2011) Purification of tubulin from porcine brain. *Methods Mol Biol* 777: 15–28.
51. Gell C, et al. (2010) Microtubule dynamics reconstituted in vitro and imaged by single-molecule fluorescence microscopy. *Methods Cell Biol* 95:221–245.
52. Mahamdeh M, Schäffer E (2009) Optical tweezers with millikelvin precision of temperature-controlled objectives and base-pair resolution. *Opt Express* 17(19): 17190–17199.